

Characterization of the RF Board for microwave SQUID multiplexing readout electronics

J. Wang,^a X. Ren^{a,1}

^aKey Laboratory of Particle Physics and Particle Irradiation (MOE),
Institute of Frontier and Interdisciplinary Science, Shandong University,
Qingdao, Shandong, 266237, China

E-mail: renxx@sdu.edu.cn

ABSTRACT: Microwave SQUID multiplexing (μ MUX) is a widely used readout technique for large-scale transition-edge sensor (TES) arrays. It uses radio-frequency (RF) probe tones to interrogate cryogenic resonators, requiring frequency conversion between the baseband electronics and the cryogenic RF signal chain. This work describes the RF Board, a room-temperature frequency-conversion board deployed in the AliCPT μ MUX readout system. The board up-converts 0–4 GHz baseband I/Q signals to the 4–8 GHz RF band for injection into the cryogenic chain and down-converts returned RF signals to baseband I/Q for ADC digitization. For the current 1000-tone operation, with a DAC output tone power of -30 dBm/tone, the required power windows are -35 to -25 dBm/tone for the RF tones transmitted to the cryostat and -45 to -35 dBm/tone at the ADC input for the returned tones. The RF Board is characterized using swept single-tone measurements covering up-conversion, down-conversion, and RF loopback. Based on these measurements, the RF output power is calculated to be -31.06 to -25.53 dBm, satisfying the RF output window. Assuming a representative cryogenic-chain transmission of -40 dB, the loopback result gives an estimated returned power of -45 to -35 dBm, within the target range. These results show that the RF Board meets the wideband frequency-conversion and tone-power requirements for the μ MUX readout system.

KEYWORDS: Cosmic microwave background; Transition-edge sensor; Microwave SQUID multiplexing; Room-temperature readout electronics; RF electronics; Frequency conversion

¹Corresponding author.

Contents

1	Introduction	1
2	RF Board Architecture	3
3	RF Board Performance	3
3.1	Up-conversion response and RF output power	4
3.2	Down-conversion response	5
3.3	RF loopback response	6
4	Conclusion	7

1 Introduction

Ground-based measurements of cosmic microwave background (CMB) polarization increasingly rely on large-scale arrays of transition-edge sensor (TES) bolometers [1–4]. As these arrays scale up, readout systems must support higher multiplexing density to reduce cryogenic wiring and thermal loading while preserving the required science performance [2, 5]. Microwave SQUID multiplexing (μ MUX) addresses this requirement by coupling TES bolometers, via RF-SQUIDs, to microwave resonators with unique resonance frequencies. Detector signals correspond to shifts in the resonator frequencies, which are read out using probe tones transmitted through a common RF feedline [6–8]. This approach has been employed for on-sky observations with the Keck Array and adopted for large-scale deployment in the Simons Observatory [9–11].

The cryogenic resonators are read out by room-temperature electronics that generate probe tones and acquire the returned signals [12]. The room-temperature electronics deployed in the AliCPT μ MUX readout chain consist of a Baseband Board, a Control Board, and an RF Board, as shown in Figure 1 [13]. The Baseband Board, based on a Xilinx ZCU111 RFSoc evaluation board, generates and acquires baseband I/Q signals. The Control Board configures the RF Board. The RF Board serves as the bridge linking the Baseband Board and the cryogenic RF signal chain. It provides bidirectional frequency conversion between the 0–4 GHz baseband I/Q signals and the 4–8 GHz RF band.

In this role, the RF Board sets the RF output power transmitted to the cryostat and the returned power sent to the ADC. These power levels are key parameters in the readout power budget, as they influence detector noise performance and readout signal-to-noise ratio (SNR). As the electronics noise floor is approximately independent of the readout-tone power, the tone power should be maximized within the linear regime of the system to improve the readout SNR. For the nominal operating condition evaluated here, a 1000-tone frequency comb spans the 4 GHz bandwidth with a baseline DAC output of -30 dBm/tone. After up-conversion, the RF tone power must be maintained within a -35 to -25 dBm/tone window. This window is set to ensure that, after approximately 45 dB

of cold attenuation, the probe-tone power at the resonator inputs falls within the optimal range of -80 to -70 dBm/tonne [7, 14, 15]. On the return path, the tones pass through cold amplifiers with a gain of about 25 dB before entering the RF Board’s receive chain, which is designed to convert and transmit the returned tones to the ADC input within a target range of -45 to -35 dBm/tonne. The main operating targets and characterization settings are summarized in Table 1.

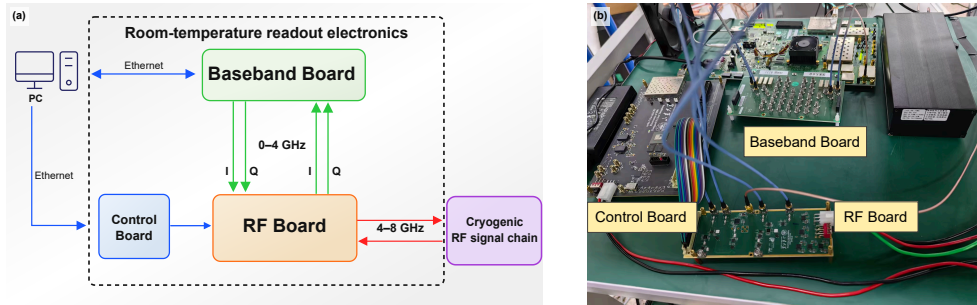


Figure 1. Room-temperature electronics in the μ MUX readout chain. (a) System block diagram of the Baseband Board, Control Board, and RF Board. (b) Photograph of the electronics system.

Table 1. Main operating targets and characterization settings for the RF Board.

Parameter	Value	Basis in this work
μ MUX RF band	4–8 GHz	Operating RF band of the cryogenic μ MUX resonators
Baseband I/Q band	0–4 GHz	Baseband frequency range supported by the DAC and ADC on the Baseband Board
Multiplexing factor	1000:1	Representative multiplexing factor used in the current μ MUX readout condition
DAC full-scale output power	+5 dBm	Typical full-scale output power of the ZCU111 RF-DAC
DAC output tone power	-30 dBm/tonne	Representative per-tone output power selected to use the available DAC dynamic range under 1000-tone operation
ADC full-scale input power	+1 dBm	Typical full-scale input power of the ZCU111 RF-ADC
Optimal resonator input tone power	-80 to -70 dBm/tonne	Optimal probe-tone power at the μ MUX resonator inputs
Required up-converted RF tone power	-35 to -25 dBm/tonne	Required RF tone power transmitted to the cryostat
Target ADC input tone power	-45 to -35 dBm/tonne	Target per-tone input power range selected to use the available ADC dynamic range under 1000-tone operation
Characterization frequency range	10 MHz–4 GHz baseband; 4.01–8 GHz RF	Set by the VNA minimum frequency of 10 MHz
Characterization frequency step	7.8125 kHz	Minimum frequency spacing supported by the Baseband Board

To verify these performance targets, swept single-tone measurements were performed on the RF Board in three configurations: up-conversion, down-conversion, and RF loopback, covering 10 MHz–4 GHz at baseband and 4.01–8 GHz in the RF band. Specifically, the up- and down-conversion routines respectively quantify the RF output power and the receive-path S_{21} response. Finally, the RF loopback setup establishes a board-level bidirectional reference to estimate the returned signal power.

2 RF Board Architecture

Functioning as the bidirectional translation interface between the baseband electronics and the cryogenic RF chain, the RF Board translates the 0–4 GHz baseband I/Q signals to the 4–8 GHz RF band to drive the cryogenic resonators, while converting the returned tones back to baseband for ADC acquisition. Figure 2 shows the architecture and hardware implementation of the RF Board. The board is organized into four functional blocks: the up-conversion path, the down-conversion path, the local oscillator (LO) module, and the power module. The LO module generates and distributes a common 4 GHz LO signal to both conversion paths and accepts an external reference input, while the power module supplies the voltages for the on-board components.

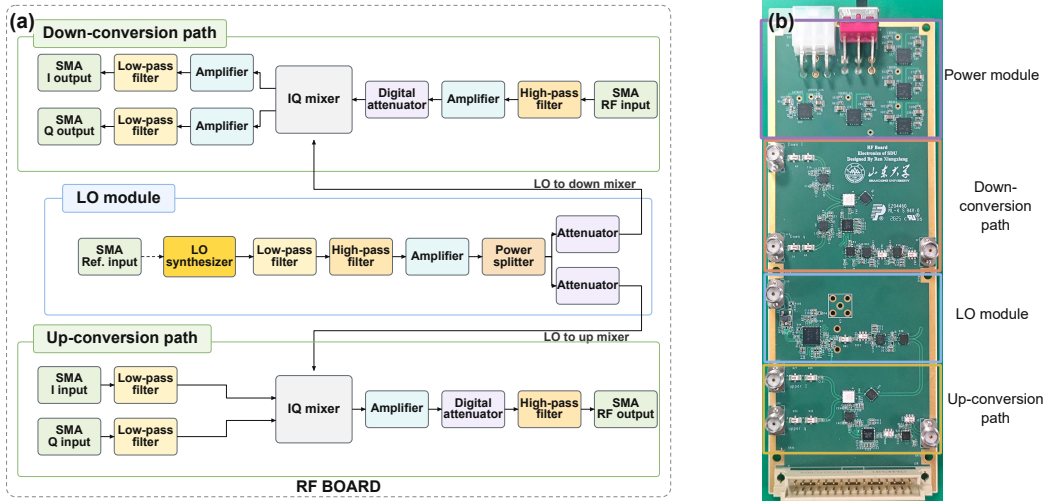


Figure 2. RF Board architecture and hardware implementation. (a) Functional block diagram showing the up-conversion path, down-conversion path, and LO module. (b) Photograph of the RF Board.

In the board implementation, the up- and down-conversion paths are realized using two Marki Microwave MMIQ-0416LSM IQ mixers. Each path incorporates programmable attenuators, fixed attenuators, amplifiers, and filters to set the path gain, adjust the tone power, and define the operating bandwidth. The shared 4 GHz LO signal is generated by a Texas Instruments LMX2595 frequency synthesizer and distributed to the two mixers through a Mini-Circuits GP2X1 power splitter.

3 RF Board Performance

To evaluate the performance of the RF Board, we performed swept single-tone measurements in three configurations: up-conversion, down-conversion, and RF loopback. In this work, the

conversion and loopback responses are reported as effective S_{21} magnitudes in dB, calculated from the corresponding output and input powers. The up-conversion measurements tested the transmit path and were used to calculate the RF output power. The down-conversion measurements characterized the receive-path response. The RF loopback measurements provided the combined bidirectional response of the RF Board, which was used as a board-level reference for estimating the returned power.

All measurements were carried out using a Keysight N5242B PNA-X vector network analyzer. The RF Board LO was set to 4 GHz and locked to the 10 MHz reference output of the VNA. Before data acquisition, the VNA was calibrated using a Keysight N4433D electronic calibration module and a Keysight U2000A power meter. This calibration corrected the test-cable losses and the relative delay between the I and Q paths, thereby moving the measurement reference planes to the cable ends connected to the RF Board. It also ensured that the swept baseband I/Q tones applied to the RF Board inputs maintained the required 90° phase relationship, consistent with the quadrature I/Q drive used in operation. The frequency sweeps covered 10 MHz–4 GHz at baseband and 4.01–8 GHz in the RF band, with a frequency step of 7.8125 kHz, matching the minimum frequency spacing supported by the Baseband Board. The characterization setup is shown in Figure 3.

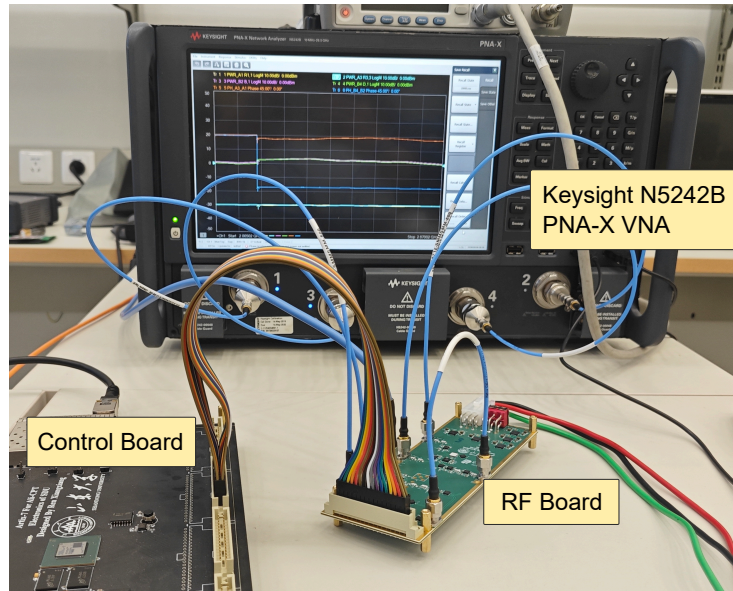


Figure 3. Measurement setup for RF Board characterization, including the Keysight N5242B PNA-X vector network analyzer, the RF Board under test, and the Control Board used to configure the RF Board.

3.1 Up-conversion response and RF output power

The up-conversion measurements were used to verify whether the transmit path provides the required RF power transmitted to the cryostat. In the current μ MUX readout configuration, the DACs on the Baseband Board generate 1000 baseband I/Q tones, each with an output power of -30 dBm/tone. The RF Board then up-converts these tones to the 4–8 GHz RF band and transmits them to the cryogenic chain. To reproduce this condition, the VNA supplied two swept single-tone signals with a 90° relative phase offset to the I and Q inputs of the RF Board, with each input power set to

–30 dBm/tone. For this path, the effective S_{21} magnitude was derived from the RF output power and the combined baseband I/Q input power, with the programmable attenuator set to three values used during laboratory operation: 6, 9, and 15 dB. At a DAC output power of –30 dBm/tone, the nominal programmable attenuation setting is 9 dB, while the 6 dB and 15 dB settings correspond to other DAC output tone-power levels.

The up-conversion response was then used to calculate the RF output power. Using the combined baseband I/Q input power of –27 dBm and the measured S_{21} magnitude range of –4.06 to 1.47 dB at the 9 dB setting, the RF output power is calculated to be –31.06 to –25.53 dBm over the operating band, as shown in Figure 4(a). This range falls within the required –35 to –25 dBm/tone window summarized in Table 1. Relative to this setting, the 6 dB setting increases the RF output power, whereas the 15 dB setting lowers it, providing a tuning range for determining the optimal drive power for the cryogenic resonators.

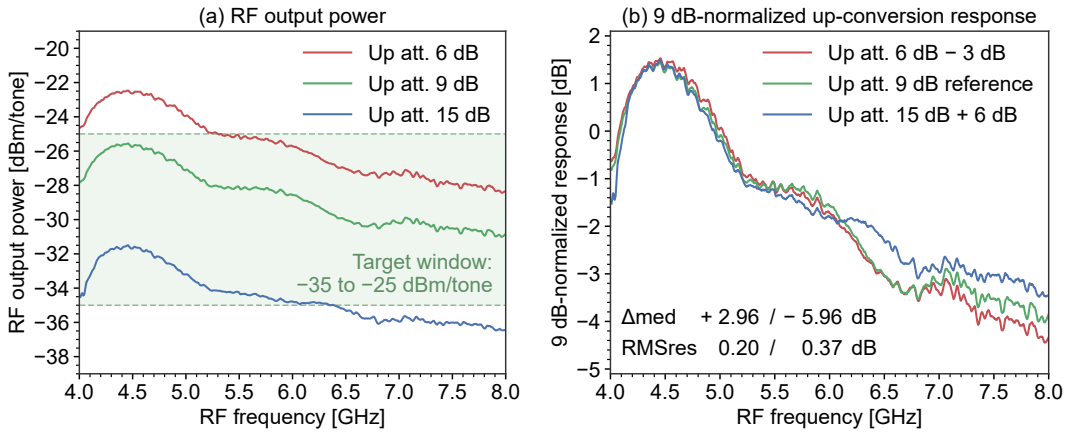


Figure 4. Up-conversion characterization. (a) RF output power calculated at the three attenuation settings. The shaded region indicates the required RF output power window of –35 to –25 dBm/tone. (b) Offset-normalized up-conversion traces referenced to the 9 dB attenuation setting.

The traces at different attenuation settings further indicate that the programmable attenuator primarily shifts the overall level while leaving the wideband shape largely unchanged. To verify the interpretation, the 6 dB and 15 dB curves were shifted by –3 dB and +6 dB, respectively, to align them with the 9 dB reference trace. After this normalization, the three curves closely overlap across most of the frequency band, as shown in Figure 4(b). The median shifts from the 9 dB reference are +2.96 dB and –5.96 dB for the 6 dB and 15 dB traces, respectively, with corresponding RMS residuals of 0.20 dB and 0.37 dB. These values indicate that the programmable attenuator provides predictable gain adjustment while largely preserving the frequency-dependent response. During system operation, the measured curve could also be used to pre-equalize the DAC tone powers, thereby reducing frequency-dependent variations in the RF output power.

3.2 Down-conversion response

The receive-path conversion response was evaluated using down-conversion measurements. The VNA supplied a swept RF tone to the board’s RF input, and the resulting baseband I/Q outputs were recorded. The down-conversion S_{21} was then derived by comparing the combined baseband I/Q

output power against the applied RF input power. These tests were performed at three representative receive-path attenuation settings: 21, 18, and 15 dB.

Figure 5(a) shows the expected dependence on the attenuation setting. Following the same normalization procedure used in Section 3.1, the three curves closely overlap, as shown in Figure 5(b). The 15 dB trace relative to the 18 dB reference gives a median shift of +3.03 dB with an RMS residual of 0.11 dB, while the 21 dB trace gives a median shift of -2.96 dB with an RMS residual of 0.06 dB. The measured shifts are consistent with the expected attenuation changes set by the receive-path programmable attenuator.

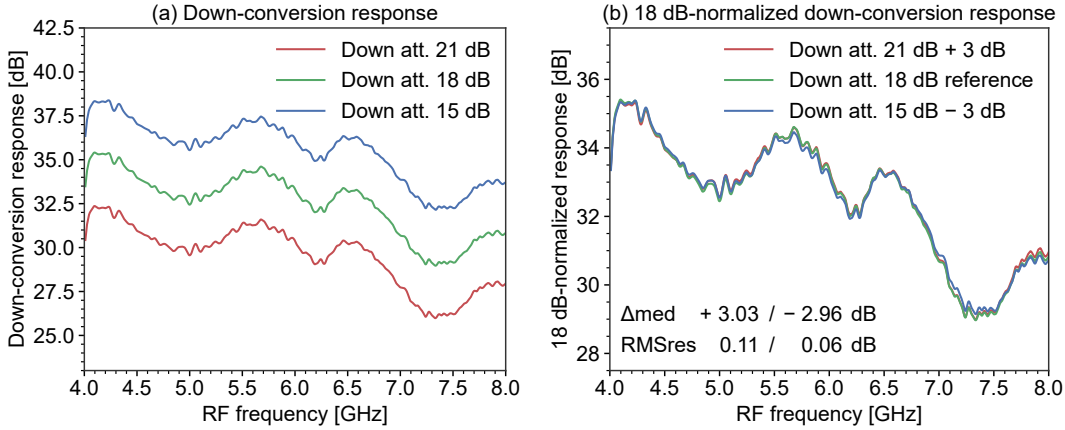


Figure 5. Down-conversion characterization. (a) Down-conversion traces at three programmable attenuation settings. (b) Offset-normalized down-conversion traces referenced to the 18 dB attenuation setting.

3.3 RF loopback response

The RF loopback measurements were used to characterize the combined behavior of the transmit and receive paths of the RF Board. For this test, the up-conversion RF output was connected directly to the down-conversion RF input. Figure 6 compares the RF loopback results for three pairs of up- and down-conversion attenuation settings: 6/21, 9/18, and 15/15 dB. The two 27 dB total-attenuation cases nearly overlap, whereas the 30 dB case shows a lower overall level.

The direct loopback result was then compared with a reconstructed result calculated as the sum of the independently obtained up- and down-conversion responses. As shown in Figure 7, the two methods match closely for all three setting pairs. The mean residuals are 0.81, 0.58, and 0.31 dB, with RMS residuals of 1.01, 0.80, and 0.68 dB for the 6/21, 9/18, and 15/15 dB setting pairs, respectively. The residual statistics indicate negligible discrepancy between the two approaches, validating the direct loopback result as the board-level reference.

After accounting for the cryogenic-chain transmission, the board-level test results can be used to evaluate the power budget at the ADC input. The cryogenic detector chain typically has a transmission of -20 to -40 dB, and -40 dB was adopted as a representative value for this estimate. For the representative 9/18 dB setting pair shown in Figure 7(b), the board-level loopback S_{21} magnitude ranges from 25 to 35 dB. When combined with the 40 dB transmission loss of the cryogenic chain, the total system S_{21} translates to -15 to -5 dB. With a DAC output tone power of

−30 dBm/tone, the corresponding power at the ADC input is −45 to −35 dBm/tone per channel, within the target range shown in Table 1. For cryogenic chains with lower attenuation, the RF Board’s programmable attenuation can be increased accordingly. As discussed in Section 3.1, pre-equalizing the DAC tone powers could further reduce variations in the returned power.

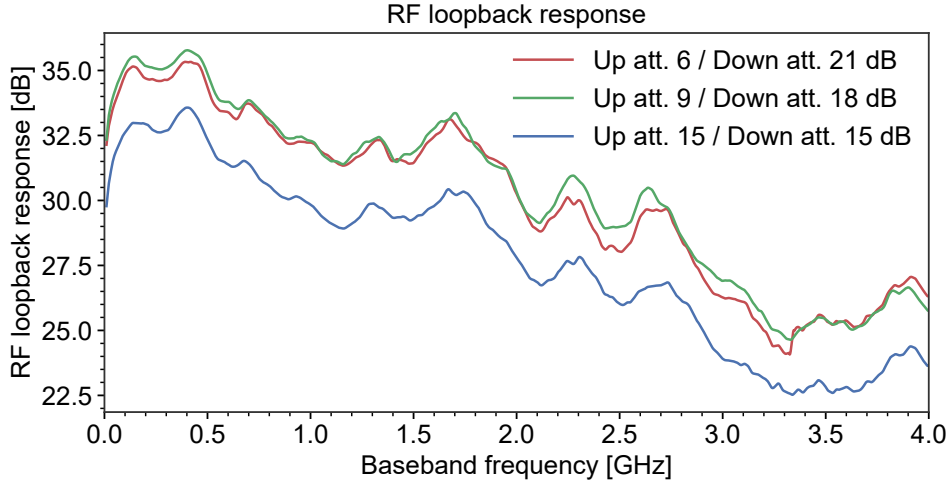


Figure 6. RF loopback responses at up/down attenuation settings of 6/21, 9/18, and 15/15 dB.

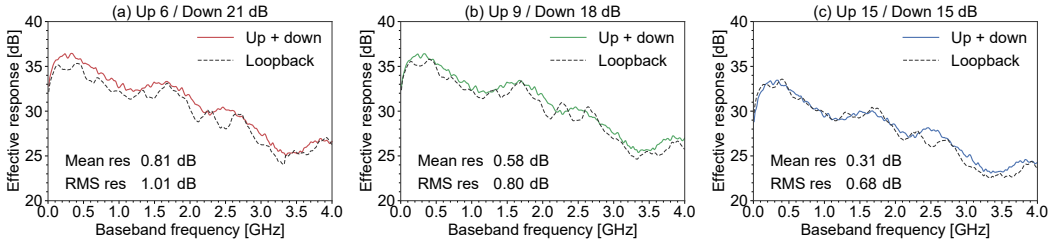


Figure 7. Comparison of the summed independently obtained up- and down-conversion curves with the directly measured RF loopback responses at up/down attenuation settings of (a) 6/21 dB, (b) 9/18 dB, and (c) 15/15 dB. The insets give the mean and RMS residuals.

Furthermore, the validated loopback S_{21} can be used as a reference to derive the effective S_{21} of the cryogenic chain. Once the cryogenic chain is connected, the measured full-link response will include both the RF Board contribution and the cryogenic-chain transmission. The effective cryogenic-chain S_{21} can then be obtained by subtracting the loopback S_{21} from the full-link response.

4 Conclusion

This work has described the RF Board used as the room-temperature bidirectional frequency conversion interface in the μ MUX readout chain. Its performance was evaluated in three configurations: up-conversion, down-conversion, and RF loopback.

The up-conversion and down-conversion measurements established the effective S_{21} of the transmit and receive paths, respectively. For both paths, the attenuation settings produced the

expected gain shifts while largely preserving the wideband shapes. The calculated RF output power ranged from -31.06 to -25.53 dBm in the current operating configuration, meeting the required power specification of -35 to -25 dBm/tone. The RF loopback measurement was shown to provide a valid board-level characterization and was used to estimate a returned power of approximately -45 to -35 dBm, which falls within the target range. Overall, these results indicate that the RF Board meets the requirements for wideband bidirectional frequency conversion and remains compatible with the power budget for the current μ MUX readout condition.

Acknowledgments

This work is supported by the National Key Research and Development Program of China (Grant No. 2022YFC2204904, No. 2020YFC2201704).

References

- [1] K.N. Abazajian et al., *CMB-S4 science book, first edition*, Tech. Rep. FERMILAB-FN-1024-A-AE, CMB-S4 Collaboration (10, 2016), [DOI](#).
- [2] M.H. Abitbol et al., *CMB-S4 technology book, first edition*, Tech. Rep. FERMILAB-FN-1034-AE, CMB-S4 Collaboration (06, 2017), [DOI](#).
- [3] K.D. Irwin and G.C. Hilton, *Transition-edge sensors*, in *Cryogenic Particle Detection*, C. Enss, ed., (Berlin Heidelberg), pp. 63–150, Springer (2005), [DOI](#).
- [4] BICEP2, KECK ARRAY AND SPIDER collaboration, *Antenna-coupled TES bolometers used in BICEP2, Keck Array, and SPIDER*, *Astrophys. J.* **812** (2015) 176 [[arXiv:1502.00619](#)].
- [5] C. Yu et al., *SLAC Microresonator RF (SMuRF) electronics: a tone-tracking readout system for superconducting microwave resonator arrays*, *Rev. Sci. Instrum.* **94** (2023) 014712 [[arXiv:2208.10523](#)].
- [6] J.A.B. Mates, G.C. Hilton, K.D. Irwin, L.R. Vale and K.W. Lehnert, *Demonstration of a multiplexer of dissipationless superconducting quantum interference devices*, *Appl. Phys. Lett.* **92** (2008) 023514.
- [7] B. Dober et al., *A microwave SQUID multiplexer optimized for bolometric applications*, *Appl. Phys. Lett.* **118** (2021) 062601 [[arXiv:2010.07998](#)].
- [8] D.T. Becker et al., *Working principle and demonstrator of microwave-multiplexing for the HOLMES experiment microcalorimeters*, *JINST* **14** (2019) P10035 [[arXiv:1910.05217](#)].
- [9] A. Cukierman et al., *Microwave multiplexing on the Keck Array*, *J. Low Temp. Phys.* **199** (2020) 858 [[arXiv:1909.01305](#)].
- [10] H. McCarrick et al., *The Simons Observatory microwave SQUID multiplexing detector module design*, *Astrophys. J.* **922** (2021) 38 [[arXiv:2106.14797](#)].
- [11] T.P. Satterthwaite et al., *The Simons Observatory: studies of detector yield and readout noise from the first large-scale deployment of microwave multiplexing at the Large Aperture Telescope*, *Proc. SPIE* **13102** (2024) 1310223 [[arXiv:2406.01844](#)].
- [12] J.D. Gard et al., *A Scalable Readout for Microwave SQUID Multiplexing of Transition-Edge Sensors*, *J. Low Temp. Phys.* **193** (2018) 485.

- [13] S.W. Henderson et al., *Highly-multiplexed microwave SQUID readout using the SLAC Microresonator Radio Frequency (SMuRF) electronics for future CMB and sub-millimeter surveys*, *Proc. SPIE* **10708** (2018) 1070819 [[arXiv:1809.03689](#)].
- [14] B. Dober et al., *Microwave SQUID multiplexer demonstration for cosmic microwave background imagers*, *Appl. Phys. Lett.* **111** (2017) 243510 [[arXiv:1710.04326](#)].
- [15] D. Dutcher et al., *The Simons Observatory: large-scale characterization of 90/150 GHz TES detector modules*, *J. Low Temp. Phys.* **214** (2024) 247 [[arXiv:2311.05583](#)].